Astrophysical reaction rates with realistic nuclear level densities

Sangeeta, A; Ghosh, T.; Maheshwari, B.; Saxena, G.; Agrawal, B. K.

Download date / Datum preuzimanja: **2024-08-16**

Repository / Repozitorij:

Repository of the Faculty of Science - University of Zagreb

Astrophysical reaction rates with realistic nuclear level densities

Sangeeta,[1] T. Ghosh,[2,3] B. Maheshwari,[4,5] G. Saxena,[6,*] and B. K. Agrawal[2,3]

[1]*Department of Applied Sciences, Chandigarh Engineering College, Landran 140307, India*
[2]*Saha Institute of Nuclear Physics, Kolkata 700064, India*
[3]*Homi Bhabha National Institute, Anushakti Nagar, Mumbai 400094, India*
[4]*Department of Physics, Faculty of Science, University of Zagreb, HR-10000 Zagreb, Croatia*
[5]*Department of Physics, Indian Institute of Technology Ropar, Rupnagar 140001, India*
[6]*Department of Physics (H & S), Government Women Engineering College, Ajmer 305002, India*

Realistic nuclear level densities (NLDs) obtained within the spectral distribution method (SDM) are employed to study nuclear processes of astrophysical interest. The merit of SDM lies in the fact that the NLDs corresponding to many-body shell-model Hamiltonians consisting of residual interaction can be obtained for the full configurational space without recourse to the exact diagnolization of huge matrices. We calculate NLDs and *s*-wave neutron resonance spacings which agree reasonably well with the available experimental data. By employing these NLDs, we compute reaction cross sections and astrophysical reaction rates for radiative neutron capture in few Fe-group nuclei and compare them with experimental data as well as with those obtained with NLDs from phenomenological and microscopic mean-field models. The results obtained for the NLDs from SDM are able to explain the experimental data quite well. These results are of particular importance since the configuration mixing through the residual interaction naturally accounts for the collective excitations. In the mean-field models, the collective effects are included through the vibrational and rotational enhancement factors, and their NLDs are further normalized at low energies with neutron resonance data.

I. INTRODUCTION

Neutron capture reactions are critical for a wide variety of applications ranging from medicine [1], energy generation [2], to nucleosynthesis [3]. Such reactions are fundamentally important by which nearly all of the elements heavier than iron are synthesized through the astrophysical *s* process or *r* process. The astrophysical site where the *r* process occurs has been one of the major open questions for the past several decades. Supernovas and neutron star mergers are the most favored astrophysical sites for the *r* process. Only recently, observations connected to the neutron star merger event GW170817 [4] have confirmed the emission of a kilonova afterglow which is powered by the radioactive decay of heavy nuclides produced in the *r* process [5,6]. Efforts are also being made to simulate the neutron capture nucleosynthesis in the laboratory [7]. This led to a rapid increase in attention on various processes contributing to nuclear reaction network.

The extensive radiative neutron capture cross-section data are crucial for complete understanding of *r*-process nuclear astrophysical network calculations. All such data are not accessible in the accelerator-based experiments, and one needs to rely on theoretical estimates. The reaction cross sections and relevant reaction rates are calculated within a statistical framework [8] which primarily requires: (i) the

neutron-nucleus optical model potential (OMP), (ii) the γ-ray strength function (γSF), and (iii) the nuclear level density (NLD). The uncertainties of γSF and NLD have significant impact on calculated neutron capture rates whereas the uncertainties due to OMP are relatively smaller [9,10]. The NLD describes the total number of states accessible in a given nucleus at a specific excitation energy. Various methods have been employed to calculate the NLDs which range from simple phenomenological models based on noninteracting degenerate Fermi gas [11,12] to more complex mean-field descriptions [13]. In the mean-field approaches, all the collective effects are incorporated in NLDs through the rotational and vibrational enhancement factors. These NLDs are further normalized with the experimental data at the neutron resonances [13]. In the shell model, the configuration mixing through the residual interaction naturally accounts for the collective excitations.

There are a few approaches to calculate the NLDs within the framework of a shell model. One of them is the shell-model Monte Carlo (SMMC) [14–19], which utilizes auxiliary fields to compute the thermal trace for the energy, and then NLDs are obtained using inverse Laplace transform. Another approach to calculate the spin- and parity-dependent shell-model level densities is developed using the spectral distribution method (SDM) [20–25]. This method allows one to incorporate the many-body effects on the wave functions appropriately and is a basis for the applications of statistical spectroscopy generated by many-body chaos as modeled by

*gauravphy@gmail.com

embedded random matrix ensembles along with the studies on β-decay rates for stellar evolution and supernovas [26–29]. Recently, the SDM has been extended for the exact calculation of the first and second Hamiltonian moments for different configurations at fixed spin and parity [30–33]. This is a practical tool to construct the NLDs for the many-body shell-model Hamiltonian using full configurational space since it avoids the diagonalization of Hamiltonian matrices of huge dimensions. This method, however, requires an accurate estimation of the shell-model ground-state energy, which is, generally, as time consuming as the full shell-model calculation. The difficulty has been overcome by using the exponential convergence method [34] or the recently developed projected configuration interaction method [35,36]. The NLDs obtained from SDM also agree reasonably with the full shell-model calculations [32]. Recently, the extrapolated Lanczos method [37] has also been developed for an accurate computation of the level densities described within the configuration space.

In the present paper, we use realistic NLDs obtained from the spectral distribution method followed by an appropriate parity equilibration scheme for pf-model space to calculate the neutron capture reaction cross sections and astrophysical reaction rates. We consider some of the (n, γ) processes consisting a few seed nuclei for the nucleosynthesis in and around the Fe group for which experimental data are available. We compare our results with those obtained with NLDs from other phenomenological and microscopic models as commonly employed.

II. NUCLEAR LEVEL DENSITIES

The NLDs are obtained using the spectral distribution method [32] applied to the shell-model Hamiltonian with a realistic residual interaction. Within the spectral distribution method, one calculates first and second moments of the Hamiltonian for the full configurational space. These moments are then used to construct the Gaussian distribution of the levels which eventually give rise to the level density. For a given isotope (Z, N), the valence nucleons can be distributed in many ways over available orbitals. Each of these configurations is known as partition p which contains $D_{\alpha p}$ many-body states with exact quantum numbers α. The states present in a given partition are distributed over some energy region as a result of interactions inside the partition. For each partition, the statistical average of an operator $\hat{O}$ over the states is defined through the corresponding trace,

$$\langle \hat{O} \rangle = \frac{1}{D_{\alpha p}} \text{Tr}^{\alpha p} \hat{O}. \tag{1}$$

In particular, the centroid energy of the partition is the first moment of the Hamiltonian,

$$E_{\alpha p} = \frac{1}{D_{\alpha p}} \text{Tr}^{\alpha p} \hat{H}. \tag{2}$$

This comes directly from the diagonal elements of the Hamiltonian matrix. The second moment of the Hamiltonian,

$$\sigma_{\alpha p}^2 = \langle H^2 \rangle_{\alpha p} - E_{\alpha p}^2 = \frac{1}{D_{\alpha p}} \text{Tr}^{\alpha p} H^2 - E_{\alpha p}^2 \tag{3}$$

is determined by the off-diagonal elements of the Hamiltonian matrix including the interaction between partitions. No matrix diagonalization is required as this quantity can be read directly from the Hamiltonian matrix. The actual distributions are close to the Gaussians which is a manifestation of quantum complexity and chaotization [38–41]. Finally, the level density $\rho(E; \alpha)$ is found by summing the Gaussians weighted over their dimensions for all partitions at given energy E and with quantum numbers α,

$$\rho(E; \alpha) = \sum_p D_{\alpha p} G_{\alpha p}(E). \tag{4}$$

The best results are obtained by using finite range or truncated Gaussians,

$$G_{\alpha p}(E) = G(E - E_{\alpha p} + E_{\text{g.s.}}; \sigma_{\alpha p}) \tag{5}$$

for each partition. Removing unphysical tails, the Gaussians are cut off at a distance $\approx 2.6\sigma_{\alpha p}$ from the corresponding centroid and then renormalized [32]. The ground-state energies $E_{\text{g.s.}}$ appearing in Eq. (5) must be calculated using the full Hamiltonian matrix in order to be consistent with the first and second moments. Practically, it is convenient to calculate the invariant traces in the M scheme. When $\rho(E; M)$ for a given parity is computed, the level-density $\rho(E; J)$ for certain spin J is found as the difference of $\rho(M = J)$ and $\rho(M = J + 1)$.

To illustrate, we have considered the reaction cross sections for ^{50}V(n, γ) ^{51}V, ^{54}Fe(n, γ) ^{55}Fe, and ^{58}Ni(n, γ) ^{59}Ni processes. In addition to emission of γ, contributions from the ejection of neutron (n) and proton (p) are also included. This leads to the possible reaction channels, namely, (n, γ), (n, n), (n, p), $(n, 2n)$, (n, np), and $(n, 2p)$ which require the computation of NLDs for 18 nuclei, six for each process. For these nuclei, we compute NLDs with pf-model space assuming ^{40}Ca as a core. We use the GXPF1A residual interaction [42] which is well known to reproduce the binding energies, electromagnetic moments, and transitions as well as excitation spectra for pf-shell nuclei.

It may be pointed out that even a smaller inaccuracy in $E_{\text{g.s.}}$ (on the order of 0.5 MeV) would cause large uncertainties in NLDs ($\approx$30–20% for excitation energies $\approx$5–10 MeV) that can significantly affect the reaction cross sections and astrophysical reaction rates. The accurate values of $E_{\text{g.s.}}$ for the case of the pf-model space are calculated using NushellX@MSU [43]. The calculation of $E_{\text{g.s.}}$ turns out to be cumbersome in a few cases due to a large dimension corresponding to full model space (N_{full}) of the Hamiltonian matrix. In such cases, we recourse to the exponential convergence method [34]. The ground-state energies obtained for several restricted model spaces are fitted to the exponential function of the form $a + be^{-cN}$. Once the parameters a, b, and c are known, the exponentially converged value of $E_{\text{g.s.}}$ for the pf-model space can be obtained with $N = N_{\text{full}}$. For instance, in Fig. 1, the values of $E_{\text{g.s.}}$ with different truncations are plotted for ^{51}V, ^{55}Fe, and ^{59}Ni. We have also performed full model space calculations for $E_{\text{g.s.}}$ with a full JT-space dimension (N_{full}) $\lesssim 5 \times 10^6$. The exponentially converged values for $E_{\text{g.s.}}$ are found to be accurate within 0.1 MeV. In Table I, we list the values of $E_{\text{g.s.}}$ along with N_{full} for the pf-model
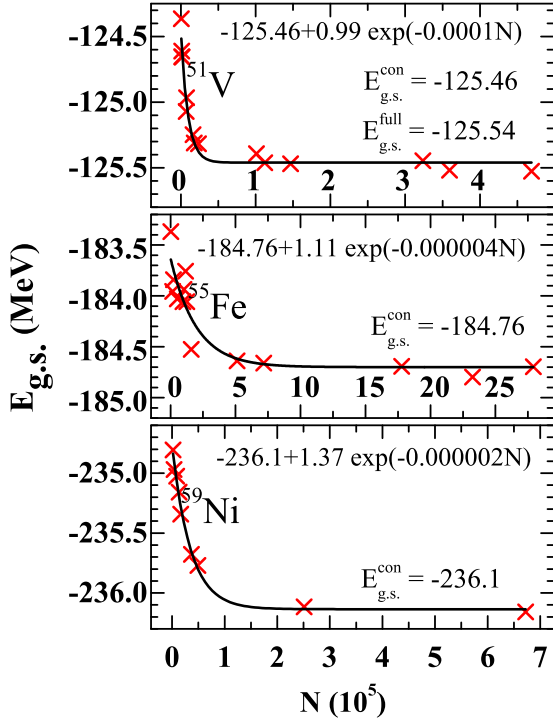
FIG. 1. Shell-model ground-state energies for ^{51}V, ^{55}Fe, and ^{59}Ni corresponding to different truncations with dimensions N (red crosses). These energies are fitted to $a + be^{-cN}$ as indicated by the solid line. The exponential converged ground-state energies for full pf-model space are obtained using this fitted expression with $N = N_{\text{full}}$.

space for all the 18 nuclei relevant to the present paper. Once the ground-state energies are known, the NLDs are calculated within the SDM using the MM code [32].

The NLDs for both parities would require the model space consisting of single-particle states with different parities. The pf-model space can yield the NLDs only for a single parity for a given nucleus. In even-A nuclei, it will correspond to only positive-parity states, and those for odd-A nuclei to the negative-parity states. Recently, Ormand and Brown [37] have estimated the values of s-wave resonance spacing D_0 for ^{57}Fe using the NLDs for $1/2^-$ states, instead of $1/2^+$

states, obtained within the pf-model space. The values of D_0 so determined agreed reasonably with the experimental data. It was, thus, inferred that the parity equilibration for ^{57}Fe occurs near neutron separation energy (S_n). The NLDs for $J^\pi = 2^+$ and 2^- states extracted from the measurements of quadrupole giant resonances in ^{58}Ni [48] showed that parity equilibration takes place at lower energy than the predictions of SMMC calculations for the $pfg_{9/2}$ model space [16,17]. Similar conclusions were also drawn on the basis of calculations performed for sufficiently large model space [49,50]. A simple formula [51] further suggested the parity equilibration to occur exponentially with an increase in temperature. We construct the level density for positive (negative) parity for an odd (even) nucleus through the parity equilibration. We use a simple scheme for the parity equilibration such as

$$\frac{\rho_+(E_x)}{\rho_-(E_x)} = \frac{1}{1 + e^{-\beta(E_x - E_0)}}, \tag{6}$$

where $\rho_+(E_x)$ and $\rho_-(E_x)$ are the level densities of positive and negative parities at excitation energy E_x for odd-A nuclei. The ρ_+ and ρ_- will be reversed for the case of even-A nuclei. The parameters β and E_0 can be adjusted to obtain required excitation energy dependence of the parity equilibration. For simplicity, we consider $\beta = 1$. We obtain the NLDs using SDM with the pf-model space by considering above parity equilibration scheme for $E_0 = S_n$ and $0.8S_n$, labeled by SDM and SDM*, respectively. These NLDs are employed to calculate the D_0, cross sections, and reaction rates.

In Fig. 2, we show the shell-model NLDs, labeled as SDM and SDM* for ^{51}V, ^{55}Fe, and ^{59}Ni nuclei as representative examples and compare them with the existing experimental data [44–46]. The NLDs obtained from the low-lying experimental discrete levels [47] are also shown for comparison. Our calculated NLDs are in an overall agreement with the experimental data for all the three nuclei. For the comparison, we also display the NLDs obtained from the HFB approach for the Skyrme-type effective force BSk14 [13]. These NLDs are obtained using combinatorial method at lower excitation energies and using the statistical method at higher excitation energies. The HFB results are further normalized to the experimental data at low energies and the neutron separation energy [13]. We also display un-normalized HFB results as labeled by HFB-u. The NLDs for HFB-u deviate noticeably

TABLE I. The ground-state energies $E_{\text{g.s.}}$ (MeV) for different nuclei required to compute the cross sections for the (n, γ) processes considered. The $E_{\text{g.s.}}$ are obtained using the shell-model Hamiltonian with the GXPF1A residual interaction. The exponential convergence [34] is used for the cases where the full JT-space dimension (N_{full}) exceeds $\approx 5 \times 10^6$. The exponential converged value for ^{51}V is -125.46 MeV which is nearly equal to -125.54 MeV obtained for full model space calculation ($E_{\text{g.s.}}^{\text{full}}$).

| Channels	^{50}V(n, γ) ^{51}V			^{54}Fe(n, γ) ^{55}Fe			^{58}Ni(n, γ) ^{59}Ni		
	Nucleus	N_{full}	$E_{\text{g.s.}}$	Nucleus	N_{full}	$E_{\text{g.s.}}$	Nucleus	N_{full}	$E_{\text{g.s.}}$
(n, γ)	^{51}V	1242538	-125.54	^{55}Fe	25743302	-184.76	^{59}Ni	76528736	-236.37
(n, n)	^{50}V	795219	-114.79	^{54}Fe	5220621	-175.73	^{58}Ni	21977271	-227.59
(n, p)	^{50}Ti	39899	-109.86	^{54}Mn	17069465	-167.40	^{58}Co	37534140	-218.90
$(n, 2n)$	^{49}V	422870	-105.63	^{53}Fe	21131892	-162.56	^{57}Ni	76528736	-215.55
(n, np)	^{49}Ti	150632	-99.24	^{53}Mn	14123745	-158.51	^{57}Co	90369789	-210.34
$(n, 2p)$	^{49}Sc	28603	-90.41	^{53}Cr	3776746	-151.70	^{57}Fe	13436903	-203.30
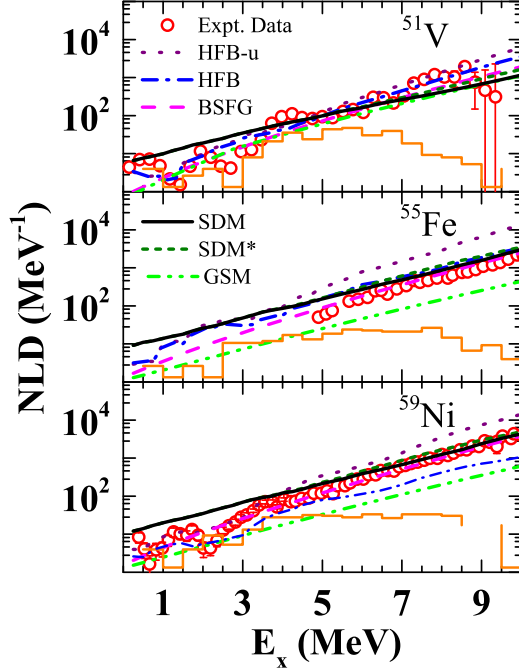
FIG. 2. Nuclear level densities as a function of excitation energies (E_x) for ^{51}V, ^{55}Fe, and ^{59}Ni nuclei obtained from SDM in the pf-model space by considering the parity equilibration scheme [given by Eq. (6)] at $E_0 = S_n$ and $0.8S_n$ labeled as SDM and SDM*, respectively. These results are compared with the experimental data [44–46] along with other microscopic mean-field models, HFB-u (un-normalized) and HFB as well as the phenomenological models, BSFG and GSM. Histograms represent the NLDs obtained from low-lying discrete levels [47].

for ^{55}Fe and ^{59}Ni nuclei. The curves marked by BSFG and GSM correspond to the phenomenological back-shifted Fermi gas model [11] and the generalized superfluid model [52,53], respectively.

The cross sections and reaction rates, relevant to the astrophysical process are predominantly governed by the NLDs corresponding to spin and parity which determines the level spacings D_0 for s-wave neutron resonance. The D_0 can be

evaluated as [13]

$$
D_0 = \begin{cases} \dfrac{1}{\rho(S_n, J_t+1/2, \pi_t) + \rho(S_n, J_t-1/2, \pi_t)} & \text{for } J_t \neq 0, \\[3mm] \dfrac{1}{\rho(S_n, 1/2, \pi_t)} & \text{for } J_t = 0, \end{cases} \tag{7}
$$

where J_t and π_t are the spin and parity of the target nucleus and S_n is the neutron separation energy for the product nucleus. It is evident from Eq. (7) that the calculation of D_0 for the even-even target nucleus requires the level density for $1/2^+$ in the product nucleus. Similarly, if the target is not even-even then the level densities for the product nucleus are required for the spins $J_t \pm 1/2$ and parity π_t. The values of D_0 are calculated using shell-model level densities with the pf-model space assuming the parity equilibration scheme [Eq. (6)] for $E_0 = S_n$ and $0.8S_n$ as listed in Table II along with the available experimental data [47]. The calculations involve NLDs from $1/2^+$ states for all the nuclei presented in Table II except for ^{50}Ti and ^{51}V. The values of D_0 for ^{50}Ti (^{51}V) include the contribution from 3^- and 4^- ($11/2^+$ and $13/2^+$) spins since $J_t^\pi \neq 0$ for these cases. The calculated values of D_0 with $E_0 = 0.8S_n$ (SDM*) are in overall agreement with the corresponding experimental data. The exceptionally larger calculated value of D_0 for ^{49}Ti requires further detailed investigation. However, NLDs for this nucleus contribute to the (n, np) channel in the neutron capture by ^{50}V which is not a dominant one. For comparison, we display the results for D_0 obtained using some selected microscopic mean-field and phenomenological models.

III. (n, γ) CROSS SECTIONS AND ASTROPHYSICAL REACTION RATES

The (n, γ) reaction cross sections are calculated using the TALYS 1.95 computer code [67] which takes into account the contributions from three major nuclear reaction mechanisms that include direct reaction, preequilibrium emission, and compound nucleus. The parameters required for cross-section calculations, such as the nuclear masses, discrete levels, decay schemes, OMP, and γSF are set to their default values available in TALYS. The extensive database for the NLDs obtained for various phenomenological and

TABLE II. The values of s-wave neutron resonances (D_0) are calculated for pf-model space considering parity equilibration scheme [given by Eq. (6)] at $E_0 = S_n$ and $0.8S_n$, labeled by SDM and SDM*. These results are compared with the experimental data along with other microscopic mean-field models, Hartree-Fock-Bogoliubov (HFB)-u (un-normalized) and HFB as well as the phenomenological models, back-shifted Fermi gas model (BSFG) and generalized superfluid model (GSM). The neutron separation energy S_n for the product nuclei and the angular momentum $J_t^{\pi_t}$ for the target nuclei are listed.

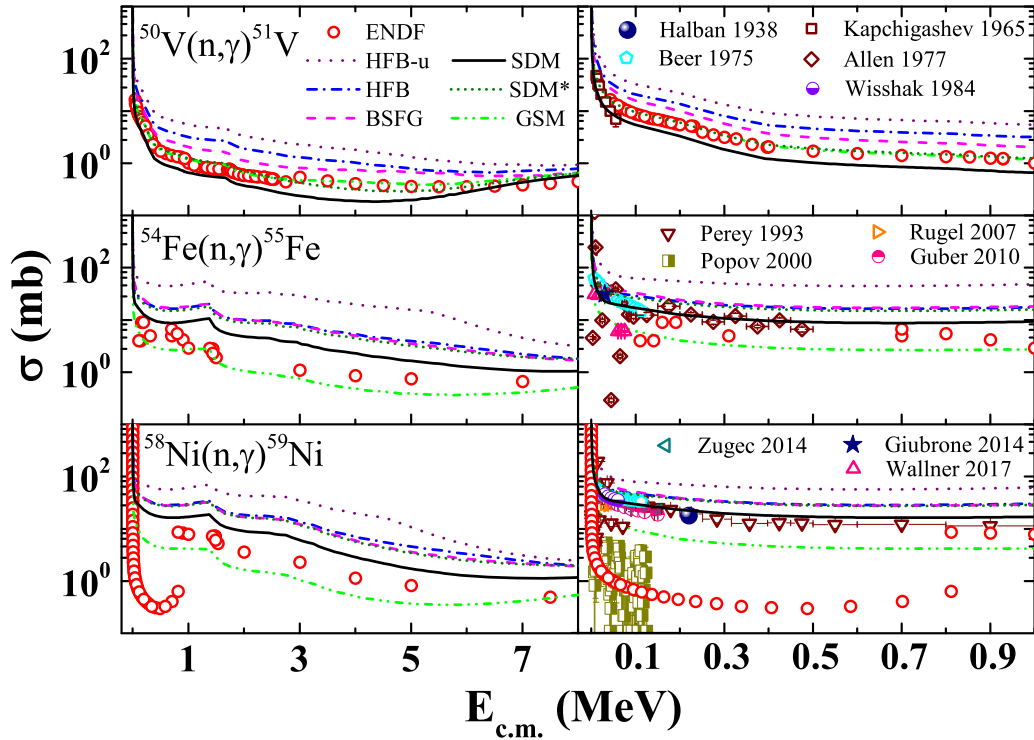| Nucleus	$J_t^{\pi_t}$	S_n (MeV)	D_0 (keV)						
			Expt.	HFB-u	HFB	BSFG	GSM	SDM	SDM*
^{49}Ti	0^+	8.142	18.3 ± 2.9	24.6	18.6	19.1	15.2	174.4	104.9
^{50}Ti	$\frac{7}{2}^-$	10.939	4 ± 0.8	1.1	4	4.1	5.2	19.6	10.8
^{51}V	6^+	11.051	2.3 ± 0.6	0.9	1.5	2.8	4.8	6.2	3.5
^{53}Cr	0^+	7.939	43.4 ± 4.4	30.1	47.7	43	79	66.2	38.4
^{55}Fe	0^+	9.298	18 ± 2.4	5.5	15.9	16.3	104	31.7	18.4
^{57}Fe	0^+	7.646	25.4 ± 2.2	22	26.4	24.5	54.2	34.8	21.2
^{59}Ni	0^+	8.999	13.4 ± 0.9	6.1	12.8	14.1	95.7	23.8	13.9

FIG. 3. Cross sections for (n, γ) processes as a function of incident neutron energies in center-of-mass frame ($E_{c.m.}$) calculated using NLDs from SDM and SDM* compared with those obtained from other models (as shown in Fig. 2), see the text for details. Evaluated data are adopted from evaluated nuclear data files (ENDF) [54]. The cross sections at low $E_{c.m.}$ are shown in the right panels together with the respective experimental data as Kapchigashev [55] for ^{50}V(n, γ) ^{51}V, Beer and Spencer [56], Allen *et al.* [57], Giubrone *et al.* [58], Wallner *et al.* [59] for ^{54}Fe(n, γ) ^{55}Fe, and Halban and Kowarski [60], Beer and Spencer [56], Wisshak *et al.* [61], Perey *et al.* [62], Popov *et al.* [63], Rugel *et al.* [64], Guber *et al.* [65], and Žugec *et al.* [66] for ^{58}Ni(n, γ) ^{59}Ni.

microscopic mean-field models are also available in TALYS. These models are the BSFG [11], the Gilbert and Cameron model [12], the GSM [52,53], the Hartree-Fock for Skyrme-type interaction with pairing treated within the Bardeen-Cooper-Schrieffer approximation [68], and the HFB for Skyrme forces [13]. We compare the reaction cross sections and astrophysical reaction rates obtained for some of these NLDs with the ones calculated using NLDs from SDM. The cross sections for ^{50}V(n, γ) ^{51}V, ^{54}Fe(n, γ) ^{55}Fe, and ^{58}Ni(n, γ) ^{59}Ni reactions are calculated by including various channels as listed in Table I. Contributions from other channels which include (α), deutron (d), tritium (t), and helium-3 (^{3}He) are found to be insignificant (not shown).

In Fig. 3, we display our theoretical estimates of (n, γ) cross sections obtained from SDM NLDs corresponding to $E_0 = S_n$ and $0.8S_n$ [Eq. (6)] and compare them with those obtained for NLDs from other models along with the evaluated data adopted from the ENDF database (ENDF/B-VII.1) [54]. In the left panels, the results are presented for a wide range of incident neutron energy. The corresponding zoomed versions for the lower energies up to 1 MeV, relevant to astrophysical reaction rates at temperatures up to the order of gigakelvins, are presented in the right panels. The cross sections based on the NLDs from SDM are in an overall agreement with the evaluated data (left panels) as well as available experimental data from various groups (right panels) [55–66]. For the low incident neutron energies, our SDM results are in

agreement with the experimental data which emphasize the role of residual interaction in the astrophysical regime. Also, the results from HFB, BSFG, and GSM are found to be in reasonable agreement with the experimental cross sections as the NLDs for these models are appropriately normalized with the measured ones. However, the results obtained by HFB-u, which correspond to un-normalized NLDs, show noticeable deviations from the measured cross sections for neutron capture reactions.

For the reaction network, one needs astrophysical reaction rates as one of the inputs. Once the variation of the cross section with energy is known, the astrophysical reaction rates $N_A \langle \sigma v \rangle$ can be computed with N_A being the Avogadro number and $\langle \sigma v \rangle$ is the Maxwellian average, where v is the relative velocity of neutron. These averages are computed at a fix temperature which ranges from 0.1 to 10 GK. For these temperatures, cross sections at energies within the range of few keV to ≈ 1 MeV contribute maximally. We show in Fig. 4, the astrophysical reaction rates obtained by using the NLDs from SDM and compare them with the recommended values from ENDF [54] and KADONIS v0.3' [69]. These results are basically the Maxwellian average of cross sections shown in Fig. 3. The results from HFB, BSFG, and GSM are also shown for comparison. SDM results with $0.8S_n \leqslant E_0 \leqslant S_n$ explain quite well the recommended values from ENDF [54] in all cases.
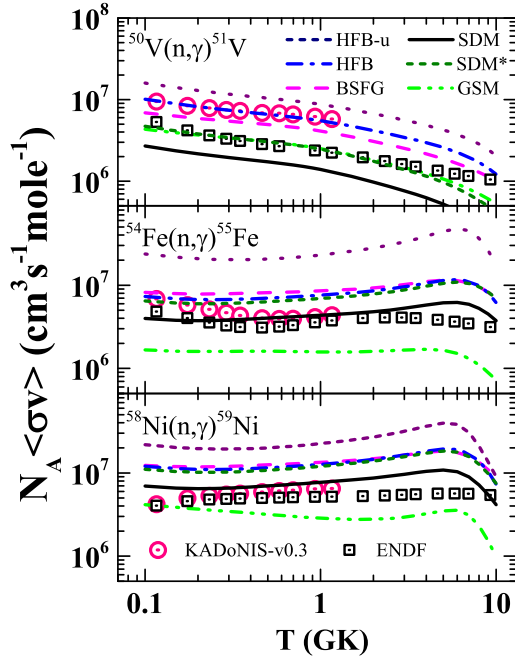
FIG. 4. The astrophysical reaction rates as a function of temperature using NLDs from SDM and SDM* compared with those obtained for other models (as shown in Fig. 2). For comparison, the recommended values from ENDF [54] and "KADONIS v0.3" [69] are shown. For the case of $^{50}V(n, \gamma)$ ^{51}V, KADONIS estimates are purely theoretical.

IV. SUMMARY AND OUTLOOK

We obtain realistic NLDs within the framework of the spectral distribution method applied to the many-body shell-model Hamiltonian for the pf-model space. Particular attention has been paid to calculate the accurate ground-state energy since it is a crucial input in the SDM calculations. To incorporate the NLDs of opposite parities in the pf-model space, an appropriate parity equilibration scheme has been used. The NLDs so obtained and s-wave neutron resonance spacings agree reasonably well with the available experimental data. We further compute reaction cross sections and astrophysical reaction rates for the neutron capture processes, such as $^{50}V(n, \gamma)$ ^{51}V, $^{54}Fe(n, \gamma)$ ^{55}Fe, and $^{58}Ni(n, \gamma)$ ^{59}Ni. The calculated reaction cross sections are found to be in harmony with experimental data, particularly, for the incident neutron energies of astrophysical interest. Similar is the case for the astrophysical reaction rates for the temperature ranging from 0.1 to 10 GK.

Since the present method is quite general and naturally accounts for the collective excitations, therefore, it can be explored in various model spaces and other reactions of astrophysical interest. To obtain the realistic shell-model NLDs of both parities naturally, it would be desirable to perform calculations with larger model spaces which involve huge computation. It would be worthwhile to study the astrophysical reaction rates using shell-model NLDs for the neutron-rich nuclei away from the line of β stability where the level density may deviate significantly compared to the nearby stable nuclei [9,70,71]. Experiments along this direction using inverse kinematics at radioactive ion-beam facilities are expected to be operational in the near future.

[1] J. J. P. de Lima, Eur. J. Phys. **19**, 485 (1998).

[2] M. Prelas, M. Boraas, F. D. L. Torre Aguilar, J.-D. Seelig, M. T. Tchouaso, and D. Wisniewski, *Nuclear Batteries and Radioisotopes* (Springer, Cham, 2016).

[3] E. M. Burbidge, G. R. Burbidge, W. A. Fowler, and F. Hoyle, Rev. Mod. Phys. **29**, 547 (1957).

[4] B. P. Abbott, R. Abbott, T. D. Abbott, F. Acernese, K. Ackley, C. Adams, T. Adams, P. Aesso, R. X. Adhikari, V. B. Adya *et al.* (LIGO Scientific Collaboration and Virgo Collaboration), Phys. Rev. Lett. **119**, 161101 (2017).

[5] I. Arcavi *et al.*, Nature (London) **551**, 64 (2017).

[6] E. Pian *et al.*, Nature (London) **551**, 67 (2017).

[7] P. Hill and Y. Wu, Phys. Rev. C **103**, 014602 (2021).

[8] W. Hauser and H. Feshbach, Phys. Rev. **87**, 366 (1952).

[9] S. N. Liddick, A. Spyrou, B. P. Crider, F. Naqvi, A. C. Larsen, M. Guttormsen, M. Mumpower, R. Surman, G. Perdikakis, D. L. Bleuel, A. Couture, L. Crespo Campo, A. C. Dombos,

R. Lewis, S. Mosby, S. Nikas, C. J. Prokop, T. Renstrom, B. Rubio, S. Siem, and S. J. Quinn, Phys. Rev. Lett. **116**, 242502 (2016).

[10] S. Dutta, G. Gangopadhyay, and A. Bhattacharyya, Phys. Rev. C **94**, 054611 (2016).

[11] W. Dilg, W. Schantl, H. Vonach, and M. Uhl, Nucl. Phys. **A217**, 269 (1973).

[12] A. Gilbert and A. G. W. Cameron, Can. J. Phys. **43**, 1446 (1965).

[13] S. Goriely, S. Hilaire, and A. J. Koning, Phys. Rev. C **78**, 064307 (2008).

[14] C. W. Johnson, S. E. Koonin, G. H. Lang, and W. E. Ormand, Phys. Rev. Lett. **69**, 3157 (1992).

[15] G. H. Lang, C. W. Johnson, S. E. Koonin, and W. E. Ormand, Phys. Rev. C **48**, 1518 (1993).

[16] H. Nakada and Y. Alhassid, Phys. Rev. Lett. **79**, 2939 (1997).

[17] H. Nakada and Y. Alhassid, Phys. Lett. B **436**, 231 (1998).

[18] H. Nakada and Y. Alhassid, Phys. Rev. C **78**, 051304(R) (2008).

[19] Y. Alhassid, M. Bonett-Matiz, S. Liu, and H. Nakada, Phys. Rev. C **92**, 024307 (2015).

[20] F. Chang, J. French, and T. Thio, Ann. Phys. (NY) **66**, 137 (1971).

[21] J. B. French and K. F. Ratcliff, Phys. Rev. C **3**, 94 (1971).

[22] V. K. B. Kota and K. Kar, Pramana **32**, 647 (1989).

[23] V. Kota and D. Majumdar, Nucl. Phys. A**604**, 129 (1996).

[24] M. Horoi, J. Kaiser, and V. Zelevinsky, Phys. Rev. C **67**, 054309 (2003).

[25] M. Horoi, M. Ghita, and V. Zelevinsky, Phys. Rev. C **69**, 041307(R) (2004).

[26] K. Kar, A. Ray, and S. Sarkar, Astrophys. J. **434**, 662 (1994).

[27] V. K. B. Kota and D. Majumdar, Z. Phys. A: Hadrons Nucl. **351**, 377 (1995).

[28] J. Gómez, K. Kar, V. Kota, R. Molina, A. Relaño, and J. Retamosa, Phys. Rep. **499**, 103 (2011).

[29] V. K. B. Kota and N. D. Chavda, Int. J. Mod. Phys. E **27**, 1830001 (2018).

[30] R. A. Sen'kov and M. Horoi, Phys. Rev. C **82**, 024304 (2010).

[31] M. Horoi and R. Senkov, PoS **NIC XI**, 222 (2011).

[32] R. Sen'kov, M. Horoi, and V. Zelevinsky, Comput. Phys. Commun. **184**, 215 (2013).

[33] R. Sen'kov and V. Zelevinsky, Phys. Rev. C **93**, 064304 (2016).

[34] M. Horoi, B. A. Brown, and V. Zelevinsky, Phys. Rev. C **65**, 027303 (2002).

[35] Z.-C. Gao and M. Horoi, Phys. Rev. C **79**, 014311 (2009).

[36] Z.-C. Gao, M. Horoi, and Y. S. Chen, Phys. Rev. C **80**, 034325 (2009).

[37] W. E. Ormand and B. A. Brown, Phys. Rev. C **102**, 014315 (2020).

[38] K. Mon and J. French, Ann. Phys. (NY) **95**, 90 (1975).

[39] T. A. Brody, J. Flores, J. B. French, P. A. Mello, A. Pandey, and S. S. M. Wong, Rev. Mod. Phys. **53**, 385 (1981).

[40] S. Wong, *Nuclear Statistical Spectroscopy* (Oxford University Press, New York, 1986).

[41] V. K. B. Kota and R. ul. Haq, *Spectral Distributions in Nuclei and Statistical Spectroscopy* (World Scientific, Singapore, 2010).

[42] M. Honma, T. Otsuka, B. A. Brown, and T. Mizusaki, Phys. Rev. C **69**, 034335 (2004).

[43] B. Brown and W. Rae, Nucl. Data Sheets **120**, 115 (2014).

[44] A. C. Larsen, R. Chankova, M. Guttormsen, F. Ingebretsen, S. Messelt, J. Rekstad, S. Siem, N. U. H. Syed, S. W. Ødegård, T. Lönnroth, A. Schiller, and A. Voinov, Phys. Rev. C **73**, 064301 (2006).

[45] A. P. D. Ramirez, A. V. Voinov, S. M. Grimes, Y. Byun, C. R. Brune, T. N. Massey, S. Akhtar, S. Dhakal, and C. E. Parker, Phys. Rev. C **92**, 014303 (2015).

[46] A. V. Voinov, S. M. Grimes, C. R. Brune, T. Massey, and A. Schiller, EPJ Web Conf. **21**, 05001 (2012).

[47] R. Capote, M. Herman, P. Obložinský, P. Young, S. Goriely, T. Belgya, A. Ignatyuk, A. Koning, S. Hilaire, V. Plujko *et al.*, Nucl. Data Sheets **110**, 3107 (2009).

[48] Y. Kalmykov, C. Özen, K. Langanke, G. Martínez-Pinedo, P. von Neumann-Cosel, and A. Richter, Phys. Rev. Lett. **99**, 202502 (2007).

[49] D. Mocelj, T. Rauscher, G. Martínez-Pinedo, K. Langanke, L. Pacearescu, A. Faessler, F.-K. Thielemann, and Y. Alhassid, Phys. Rev. C **75**, 045805 (2007).

[50] K. Van Houcke, S. M. A. Rombouts, K. Heyde, and Y. Alhassid, Phys. Rev. C **79**, 024302 (2009).

[51] Y. Alhassid, G. F. Bertsch, S. Liu, and H. Nakada, Phys. Rev. Lett. **84**, 4313 (2000).

[52] A. V. Ignatyuk, K. K. Istekov, and G. N. Smirenkin, Sov. J. Nucl. Phys. **29**, 450 (1979).

[53] A. V. Ignatyuk, J. L. Weil, S. Raman, and S. Kahane, Phys. Rev. C **47**, 1504 (1993).

[54] Evaluated Nuclear Data Files (ENDF/B-VII.1), https://www-nds. iaea.org/exfor/endf.htm; https://www.nndc.bnl.gov/astro/.

[55] S. Kapchigashev, Atomnaya Energiya **19**, 294 (1965).

[56] H. Beer and R. Spencer, Nucl. Phys. A**240**, 29 (1975).

[57] B. Allen, A. de L. Musgrove, J. Boldeman, and R. Macklin, Nucl. Phys. A**283**, 37 (1977).

[58] G. Giubrone, C. Domingo-Pardo, J. Taín, C. Lederer, S. Altstadt, J. Andrzejewski, L. Audouin, M. Barbagallo, V. Bécares, F. Bečvař *et al.*, Nucl. Data Sheets **119**, 117 (2014).

[59] A. Wallner, K. Buczak, T. Belgya, M. Bichler, L. Coquard, I. Dillmann, R. Golser, F. Käppeler, A. Karakas, W. Kutschera, C. Lederer, A. Mengoni, M. Pignatari, A. Priller, R. Reifarth, P. Steier, and L. Szentmiklosi, Phys. Rev. C **96**, 025808 (2017).

[60] H. V. Halban and L. Kowarski, Nature (London) **142**, 392 (1938).

[61] K. Wisshak, F. Käppeler, G. Reffo, and F. Fabbri, Nucl. Sci. Eng. **86**, 168 (1984).

[62] C. M. Perey, F. G. Perey, J. A. Harvey, N. W. Hill, N. M. Larson, R. L. Macklin, and D. C. Larson, Phys. Rev. C **47**, 1143 (1993).

[63] Y. P. Popov, A. V. Voinov, S. S. Parzitski, N. A. Gundorin, D. G. Serov, A. P. Kobzev, and P. V. Sedyshev, Phys. At. Nucl. **63**, 525 (2000).

[64] G. Rugel, I. Dillmann, T. Faestermann, M. Heil, F. Käppeler, K. Knie, G. Korschinek, W. Kutschera, M. Poutivtsev, and A. Wallner, Nucl. Instrum. Methods Phys. Res., Sect. B **259**, 683 (2007).

[65] K. H. Guber, H. Derrien, L. C. Leal, G. Arbanas, D. Wiarda, P. E. Koehler, and J. A. Harvey, Phys. Rev. C **82**, 057601 (2010).

[66] P. Žugec, M. Barbagallo, N. Colonna, D. Bosnar, S. Altstadt, J. Andrzejewski, L. Audouin, V. Bécares, F. Bečvář, F. Belloni *et al.* (The n_TOF Collaboration), Phys. Rev. C **89**, 014605 (2014).

[67] A. Koning, S. Hilaire, and S. Goriely, TALYS-1.95 (2020), http://www.talys.eu/download-talys/.

[68] P. Demetriou and S. Goriely, Nucl. Phys. A**695**, 95 (2001).

[69] I. Dillmann, M. Heil, F. Käppeler, R. Plag, T. Rauscher, and F. Thielemann, in *Capture Gamma-Ray Spectroscopy and Related Topics: 12th International Symposium*, edited by A. Woehr and A. Aprahamian, AIP Conf. Proc. No. 819 (AIP, Melville, NY, 2006).

[70] S. I. Al-Quraishi, S. M. Grimes, T. N. Massey, and D. A. Resler, Phys. Rev. C **63**, 065803 (2001).

[71] P. Roy, K. Banerjee, T. K. Rana, S. Kundu, S. Manna, A. Sen, D. Mondal, J. Sadhukhan, M. T. Senthil Kannan, T. K. Ghosh, S. Mukhopadhyay, D. Pandit, G. Mukherjee, S. Pal, D. Paul, K. Atreya, and C. Bhattacharya, Phys. Rev. C **102**, 061601(R) (2020).